

RESEARCH ARTICLE

10.1002/2017JD026804

Key Points:

- Uncertainty in the calculated, RH-dependent, aerosol scattering coefficient increased with ambient relative humidity and growth rate, and decreasing scattering coefficient for the two algorithms studied
- The aerosol hygroscopic growth at SGP exhibited a seasonal dependence, driven mostly by change in the aerosol chemical composition
- Correlations with the aerosol optical properties show that size-related, aerosol organic composition regulates the aerosol uptake of water

Correspondence to:

A. Jefferson,
anne.jefferson@colorado.edu

Citation:

Jefferson, A., D. Hageman, H. Morrow, F. Mei, and T. Watson (2017), Seven years of aerosol scattering hygroscopic growth measurements from SGP: Factors influencing water uptake, *J. Geophys. Res. Atmos.*, 122, 9451–9466, doi:10.1002/2017JD026804.

Received 16 MAR 2017

Accepted 19 AUG 2017

Accepted article online 24 AUG 2017

Published online 11 SEP 2017

Seven years of aerosol scattering hygroscopic growth measurements from SGP: Factors influencing water uptake

A. Jefferson^{1,2} , D. Hageman^{1,2}, H. Morrow^{2,3}, F. Mei⁴ , and T. Watson⁵

¹Cooperative Institute of Research in the Environmental Sciences, University of Colorado Boulder, Boulder, Colorado, USA,

²Earth Systems Research Laboratory, National Oceanic and Atmospheric Administration, Boulder, Colorado, USA, ³Science and Technology Corporation, Boulder, Colorado, USA, ⁴Pacific Northwest National Laboratory, Richland, Washington, USA,

⁵Brookhaven National Laboratory, Upton, New York, USA

Abstract Long-term measurements of changes in the aerosol scattering coefficient hygroscopic growth at the U.S. Department of Energy Southern Great Plains site provide information on the seasonal as well as size and chemical dependence of aerosol water uptake. Annual average sub-10 μm fRH values (the ratio of aerosol scattering at 85%/40% relative humidity (RH)) were 1.78 and 1.99 for the gamma and kappa fit algorithms, respectively. The study found higher growth rates in the winter and spring seasons that correlated with a high aerosol nitrate mass fraction. fRH exhibited strong, but differing, correlations with the scattering Ångström exponent and backscatter fraction, two optical size-dependent parameters. The aerosol organic mass fraction had a strong influence on fRH. Increases in the organic mass fraction and absorption Ångström exponent coincided with a decrease in fRH. Similarly, fRH declined with decreases in the aerosol single scatter albedo. Uncertainty analysis of the fit algorithms revealed high uncertainty at low scattering coefficients and increased uncertainty at high RH and fit parameters values.

Plain Language Summary Aerosol water content influences climate by enlarging particles that then scatter more sunlight and increase cloud droplet number. This study examines the effect of aerosol chemical composition and optical properties, that denote particle size and absorption, on aerosol water uptake. The paper's focus is on data from a continental site in north central Oklahoma that is part of the Department of Energy Atmospheric Radiation Measurement network. We found the aerosol water uptake to depend strongly on the aerosol inorganic content, size, and season.

1. Introduction

Aerosol forcing of climate is largely twofold, extinction of solar radiation or direct forcing and changes in cloud droplet formation or indirect forcing. An integral factor regulating these forcings is the aerosol water content. Globally averaged, water comprises half of the aerosol mass [Textor *et al.*, 2006]. Nguyen *et al.* [2016] calculated the water ambient mass fractions across 21 continental sites to vary from 3.7% in urban Beijing to 79% in rural Finland. In a high relative humidity (RH), marine environment water can enhance the dry aerosol volume and hence optical depth by a factor of 4 [Lewis and Schwartz, 2004]. In addition to optical depth, RH-modulated aerosol water uptake impacts the aerosol size, lifetime, asymmetry parameter, and single scatter albedo. In a microphysical context, changes in relative humidity can modify the gas to aerosol partitioning of semivolatile compounds. Water also influences aqueous oxidation reactions within the aerosol, which in turn alter the aerosol mass, optical properties, and cloud droplet activation [Gund *et al.*, 1991; Lewandowski *et al.*, 2015].

Model constraint of the aerosol extinction enhancement from water uptake depends on several factors. An AeroCom comparison of aerosol forcing models found a large diversity in the predicted aerosol water content. Much of this discrepancy stems from the high variability of ambient RH and aerosol composition but also from limited data on aerosol hygroscopic growth [Kinne *et al.*, 2006; Textor *et al.*, 2006]. Field measurements of RH-dependent aerosol optical depth exemplify this variability and highlight the difficulty in modeling aerosol hygroscopic growth. Aircraft measurements of aerosol properties over a polluted, urban region during Deriving Information on Surface Conditions from Column and Vertically Resolved Observations Relevant to Air Quality (DISCOVER-AQ) attributed 88% of the extinction variability to aerosol loading at low ambient RH and only 10% to aerosol water uptake [Beyersdorf *et al.*, 2016]. However, this same study

revealed that when RH exceeded 60%, the aerosol hygroscopic growth accounted for 62% of the extinction spatial variability and 95% of the diurnal variability.

Climate models rely heavily on remote-sensing measurements for data input. In many of the remote-sensing retrievals the RH fields and aerosol hygroscopic growth are tightly coupled. Aerosol size-dependent, data products from aerosol optical depth (AOD) measurements, such as the Ångström exponent, aerosol index, and aerosol fine mode fraction, all depend on the aerosol water content. In their assessment of aerosol hygroscopic growth between remote sensing and in situ aircraft measurements *Ziemba et al.* [2013] found good agreement between vertically resolved ambient extinction from the High-Spectral Resolution Lidar and a single-parameter, empirical estimate of the hydrated nephelometer aerosol scattering coefficient. While ground-based, in situ, humidified nephelometer measurements lack vertical resolution, in a well-mixed atmosphere they can validate the column-integrated, aerosol remote sensing retrievals. More importantly, surface measurements of nephelometer scattering as a function of RH can validate model predictions and remote sensing measurements associated with seasonal changes in and cross correlations between the aerosol optical properties.

As the resolution of remote sensing measurements increases, more sophisticated and detailed probing of small-scale, atmospheric processes become possible. High RH environments, particularly in cloud outflow, have become useful to studying cloud-aerosol interactions. For these studies, high-resolution remote sensing lidars [*Yang et al.*, 2014 and *Bar-Or et al.*, 2012] and AOD from geostationary satellites [*Saide et al.*, 2014] probe small regions of the cloud edge where the RH gradient is steep. Better aerosol hygroscopic growth information would improve these algorithms as well as those that predict cloud condensation nuclei from aerosol dry extinction, AOD, or aerosol index [*Shinozuka et al.*, 2015 and *Jefferson*, 2010]. The quality of these remote sensing retrievals depends on an ability to separate meteorological fields from aerosol optical properties.

Radiative forcing model uncertainty could be significantly reduced, and remote-sensing algorithms improved with observational constraints of the aerosol water uptake. An analysis of aerosol hygroscopic growth in relation to aerosol optical and chemical properties helps improve aerosol-typing schemes that serve as input to satellite and surface AOD algorithm retrievals. In addition, algorithm tests of aerosol properties with and without column water vapor can improve model resolution that may be obscured by the temporal and spatial variations of water fields. To this end, this study presents long-term scattering hygroscopic growth measurements that provide a regional aerosol climatology that spans seasons, source emission regions, RH, and aerosol composition.

Here we present long-term measurements of aerosol scattering hygroscopic growth from the Southern Great Plains (SGP) site in Lamont, OK, operated by the Department of Energy Atmospheric Radiation Measurement (ARM) program. These are hydration measurements that scan the aerosol sample RH from low to high values, nominally 40–85%. The aerosol in this region is an aged aerosol of mostly organic composition that is weakly perturbed by urban sources [*Sherman et al.*, 2015]. Initial hygroscopic scattering enhancement measurements at the SGP site began in 1998 and have been operated near continuously to the present date. *Sheridan et al.* [2001] presented results from the first year of operation. This paper evaluates the record from 2009 to 2015, a time when the system configuration and measurement method were consistent. The overview includes the following: (1) an evaluation of the measurement uncertainty and conditions that produce the most reliable data, (2) temporal trends and variability of fRH with other aerosol optical properties and composition, and (3) a discussion on the role of aerosol phase and measurement conditions.

2. Measurements and Methods

2.1. Sampling System and Instruments

The U.S. Department of Energy, Atmospheric Radiation (ARM), Southern Great Plains (SGP) facility is located in north central Oklahoma at a latitude of 36°36'N, a longitude of 97°29'W, and an altitude of 315 m above sea level. The site is located in an agricultural region with mostly wheat, corn, alfalfa, and hay crops. The closest urban centers are Wichita, KS, 113 km north, and Oklahoma City, OK, 136 km south from the site.

The aerosol instrumentation is housed in a trailer with a community sample inlet. The aerosol inlet is a 21.4 cm ID stainless steel pipe with a rain hat. Flow through the stack is ~800 liters per minute (Lpm). Aerosol is sampled from a 244 cm long, 5.1 cm outer diameter, stainless steel tube, positioned in the

center of the larger stack. Flow through the inner tube is maintained at 150 Lpm. The flow passes through a splitter, which separates the sample flow into 5, 30 Lpm flows. One of these 30 Lpm flows passes through a switched impactor that alternates the aerosol size between sub-10 μm and sub-1 μm aerodynamic particle diameter every 30 min. Downstream of the impactors, the sample flow splits between a Radiance particle soot absorption photometer (PSAP) and two TSI (model 3563) nephelometers operated in series. Insulation, heaters, and proportional integral differential (PID) controllers regulate the RH at the base of the main aerosol sample tube, impactor inlet, and the inlet of the first nephelometer to an RH of 40% or less. *Sheridan et al.* [2001] give a detailed overview of the Aerosol Observing System instrumentation and operation.

The TSI integrating nephelometers measure the aerosol total scattering (7–170°) and backscattering (90–170°) coefficients at visible wavelengths of 450, 550, and 700 nm. The values of the aerosol absorption coefficient used in calculation of the aerosol single scattering albedo are from the Radiance PSAP, which operates at nominal wavelengths of 467, 530, and 660 nm radiation. The 530 nm absorption coefficient was wavelength corrected to 550 nm to coincide with the nephelometer scattering coefficient. Corrections based on light truncation in the nephelometer and aerosol scatter from the PSAP filter were performed [Anderson and Ogren, 1998; Bond et al., 1999 and Ogren, 2010]. Discussion of uncertainty in the nephelometer scattering coefficients and in the PSAP absorption coefficient can be found in *Anderson et al.* [1999] and *Heintzenberg et al.* [2006], *Sheridan et al.* [2005], *Virkkula et al.* [2005], and most recently in *Sherman et al.* [2015].

The Aerodyne Aerosol Chemical Speciation Mass spectrometer (ACSM) measures the nonrefractory, submicron aerosol mass concentration. The measured ion mass components are NH_4^+ , NO_3^- , SO_4^{2-} , Cl^- , and total organics. Data were screened by the aerosol mass scattering efficiency to eliminate times with low ion detection efficiency. *Parworth et al.* [2015] discuss the ACSM operation at SGP in further detail.

2.2. Humidified Nephelometer Measurements

The humidifier was designed for robust, continual operation with little technical support other than adding water to a reservoir. So to produce a dry, reference scattering coefficient yet also minimize evaporation of semivolatile compounds such as ammonium nitrate and weak organic acids, the air sample is actively dried to a maximum RH of 40% at the dry nephelometer inlet. During winter months with low dew point temperatures, the RH inside the dry nephelometer will drop as low as 5%, adding some ambiguity to the hygroscopic growth curves as weak acids volatilize and inorganic salts potentially change phase from liquid to solid.

The humidifier rests between the two nephelometers and consists of two concentric tubes with a PID controlled heater around the outer tube. Distilled water from a reservoir circulates between the outer stainless steel tube and an inner porous PTFE (polytetrafluoroethylene) tube. The RH of the sample air, flowing down the center PTFE tube, is ramped in hourly cycles with a maximum RH at the half hour. The control RH sensor (Vaisala model HMP60) is located at the exit of the humidified nephelometer. The humidifier scans the hydration branch of the aerosol scattering coefficient. Nominal RH values at the exit of humidified nephelometer cycle from 40 to 85% RH and vary with the ambient dew point. The relative humidity inside the nephelometer is calculated from the instrument dew point measured with the Vaisala RH/T sensor at the wet nephelometer exit and the internal wet nephelometer temperature. The highest relative humidity of the sample air is at the wet nephelometer exit. The system Vaisala RH/T sensors are calibrated annually on site using a Thunder Scientific Model 2500 humidity generator, calibrated to National Institute of Standards and Technology standards.

A least squares Levenburg-Marquardt algorithm fits the data to equation (1) (section 2.3), hereafter referred to as the gamma algorithm, for the 26 min scan of each aerosol size. The parameterization shown in equation (4) (section 2.3, kappa algorithm) is fit to the data using a bivariate, linear fit routine with error in both coordinates. The fit criteria limit the scans to minimum scattering coefficients of 10 Mm^{-1} , 14 or more data points, and a minimum RH between 40 and 60% for the RH scans in the humidified nephelometer.

2.3. Aerosol Scattering Hygroscopic Growth Algorithms

Past measurements of the RH dependence of the aerosol scattering coefficient date back to *Pueschel et al.* [1969] and have been done for multiple regions using varying techniques as well as equations to

parameterize the growth behavior [Covert *et al.*, 1972, Kotchenruther *et al.*, 1999, Gasso *et al.*, 2000, Quinn *et al.*, 2005, Carrico *et al.*, 2008, Fierz-Schmidhauser *et al.*, 2010, Zieger *et al.*, 2013, and Titos *et al.*, 2014]. Aerosol which are metastable or are on the upper branch of the hygroscopic growth hysteresis curve for an inorganic salt will typically follow a simple power law fit as described by Kasten [1969].

$$\sigma_w(\text{RH}_w)/\sigma_o(\text{RH}_o) = a(1 - \text{RH}_w/100)^{-\gamma} \quad (1)$$

Here γ and “ a ” are the fit parameters, and $\sigma_o(\text{RH}_o)$ is the aerosol scattering coefficient held at a reference humidity, and $\sigma_w(\text{RH}_w)$ is the scattering coefficient at a specified higher or “wet” RH. The parameter a normalizes the scattering growth, typically to an RH of 40%, and γ indicates the magnitude of the hygroscopic increase in the scattering coefficient. A common term to compare this growth across studies, geographic regions, and fit equations is fRH or the ratio of wet/dry scattering with a reference RH of 40% and a wet RH of 85%. For an ambient aerosol, fRH varies from 1.0 for hydrophobic soot aerosol to as high as ~ 4 for sea-salt aerosol [Randles *et al.*, 2004].

Brock *et al.* [2016] proposed another method to calculate the extinction hygroscopic growth that is built on a modified Köhler equation first proposed by Petters and Kreidenweis [2007] for the ambient aerosol, diameter hygroscopic growth.

$$gf(D) = \left(1 + \kappa_d \frac{\text{RH}}{100 - \text{RH}}\right)^{1/3} \quad (2)$$

Here $gf(D)$ is the hygroscopic, diameter growth. The κ_d fit parameter is tied to the average water activity of the combined, aerosol components. The aerosol scattering hygroscopic growth is derived from the cube of equation (2) or volume growth factor and the Mie scattering equation below.

$$\sigma = \int \frac{\pi}{4} D^2 Q(n, D) N(D) dD \quad (3)$$

Q is the scattering efficiency; n is the refractive index and N the number concentration. For particle sizes smaller than the wavelength of visible light used in these measurements (550 nm), changes in Q can be approximated as linear with D such that $\sigma \propto D^3$. Based on the Mie equation above, the aerosol scattering hygroscopic growth can be expressed in terms of a volume growth.

$$\frac{\sigma_w}{\sigma_d} = \left(1 + \kappa_{sca} \frac{\text{RH}}{100 - \text{RH}}\right) \quad (4)$$

The κ_{sca} of equation (4) is proportional to κ_d of equation (2) but not equivalent. Kuang *et al.* [2017] estimate $\kappa_{sca}:\kappa_d$ from a site in the North China Plains to range between 0.55 and 0.81, based on κ_d derived from measured aerosol size distributions and fRH measurements. The size-integrated κ_d and nephelometer κ_{sca} values from this study exhibited a tight linear correlation with an $r^2 = 0.97$. In addition, the ratio of $\kappa_{sca}:\kappa_d$ was found to vary with the particle size distribution with smaller particles having higher ratios. Brock *et al.* [2016] measured a similar ratio of 0.6–1.0 from their measurements in the southeastern U.S. This equation may not hold for super micron aerosol and needs evaluation in this size range.

The correlation between the two algorithms varies with RH and scattering values such that one fit equation may perform better over differing RH range, scattering coefficient, aerosol type, modal size distribution, or growth rate. The algorithm performance depends on how well the aerosol growth pattern within a given RH range conforms to the fit as well as the total fit uncertainty with respect to the combined RH and aerosol scattering uncertainties.

3. Calculation of Uncertainty

An informed use of the fRH fits requires knowledge of the fit uncertainty over a range of conditions such as loading, RH, and growth rate. The most common application of the scattering hygroscopic fit parameter in models and in instrument comparisons is the calculation of aerosol extinction or scattering at an ambient RH from the dry measurement. With this in mind, the uncertainty in the scattering

hygroscopic growth is expressed in terms of the calculated scattering coefficient at a given RH or wet scattering coefficient.

$$\sigma_w(\text{RH}_w) = \sigma_d(\text{RH}_d) \left[\frac{(1 - \frac{\text{RH}_w}{100})}{1 - \frac{\text{RH}_o}{100}} \right]^{-\gamma} \quad (5)$$

$$\sigma_w(\text{RH}_w) = \sigma_d(\text{RH}_d) \left[b + \kappa_{\text{sca}} \left(\frac{\text{RH}_w}{100 - \text{RH}_w} \right) \right] \quad (6)$$

RH_d and RH_w are the relative humidity values from the dry, reference nephelometer and ambient (wet) conditions, respectively.

Application of the fit parameters to determine an ambient scattering coefficient requires normalization to a reference scattering coefficient at a given RH_d . Both the kappa and gamma algorithms assume a continuously increasing scattering coefficient with increasing RH. The RH at which the aerosol scattering coefficient displays a measureable increase will vary with the aerosol composition and phase. We define RH_o as the maximum RH below which no measureable scattering growth with RH is observed. RH_o is set to 40% in the uncertainty calculations. We replaced the kappa fit offset value of 1 with a second fit parameter b for the kappa equation. Tying the fit to a value of 1 at $\text{RH}_w = 0$ implies a continuous growth in the scattering coefficient with RH throughout the RH range. Observations show that ambient aerosols retain some water down to low RH [Engelhart *et al.*, 2011]. Some aerosol types display an increase in scattering below 40% RH, particularly if the aerosol is highly hygroscopic. Here we use an RH of 40% as a reference RH. The reference RH can be adjusted to aerosol-specific scattering growth behavior. Note that at RH_o , $b = 1 - \kappa_{\text{sca}} (\text{RH}_o / (100 - \text{RH}_o))$ and $a = (1 - \text{RH}_o / 100)^\gamma$.

The uncertainty is determined by summing the errors of the individual sources in quadrature. We set RH_o to 40% for the uncertainty calculations. The uncertainty associated with equation (5) is given below.

$$\frac{\delta\sigma_w}{\sigma_w} = \sqrt{\left(\frac{\partial\sigma_w}{\partial\sigma_d} \delta\sigma_d \right)^2 + \left(\frac{\partial\sigma_w}{\partial\text{RH}_w} \delta\text{RH}_w \right)^2 + \left(\frac{\partial\sigma_w}{\partial\gamma} \delta\gamma \right)^2} \quad (7)$$

The uncertainty of equation (6) involves substituting κ for γ in equation (7) and adding a fourth term for uncertainty associated with the b parameter. Uncertainty in b is taken as the standard deviation of this uncertainty in fits of the data. The average standard deviation in b for the kappa fits is ± 0.035 for fits with an r^2 correlation coefficient greater than 0.3.

The uncertainty in the relative humidity measurement was taken as the reported uncertainty from Vaisala of 3%. The uncertainty in the nephelometer wet and dry scattering coefficients stems from five sources; noise, instrument drift, angular scattering truncation, calibration, and STP corrections. These uncertainties for 1 min signal integration as a function of the scattering coefficient are reported in Anderson *et al.* [1999].

The standard deviations of the fit parameters γ and κ were calculated numerically from a Monte Carlo (MC) simulation of equations (1) and (4). The kappa fit b parameter was set equal to 1 for the MC simulation in order to evaluate the role of scattering and RH on κ uncertainty and for comparison of this uncertainty with γ . In the MC simulation σ_d was varied for 1, 10, and 100 Mm^{-1} . The MC method uses random sampling to simulate the probability distribution of data about a mean value. As a first approximation, the only factors contributing to the uncertainty inputs in the simulation are the nephelometer noise and RH. We ran 1000 fit simulations for each set of input parameters using a random sequence of numbers generated over the nephelometer range of noise for a given dry scattering coefficient and a 3% uncertainty in RH.

The results of the MC simulation are given in Table 1. The γ fit values of 0.2, 0.5, and 0.8 were used in the MC simulation, which correspond to fRH (85%/40%) values of 1.3, 2.0, and 3.0, respectively. The κ fit values were set to 0.05, 0.2, and 0.4, which correspond to fRH (85%/40%) values of 1.2, 2.0, and 3.0, respectively. The MC simulation used an RH range between 40% and 85%. Using a lower or higher RH range did not significantly change the calculated uncertainty of the fit parameters. The most notable result of the simulation is the high standard deviation at low scattering coefficients. Table 1 lists the standard deviation of the calculated fit parameter in the MC simulation with fit value and scattering coefficient. Both γ and κ uncertainty values decrease

Table 1. Monte Carlo Simulated Uncertainties in Mm^{-1} for Gamma and Kappa Algorithm Fit Parameters for Dry Scattering Coefficients

Fit parameter	Scattering Coefficient (Mm^{-1})		
	1	10	100
Kappa 0.05	0.05	0.01	0.00
Kappa 0.2	0.07	0.01	0.00
Kappa 0.4	0.12	0.01	0.01
Gamma 0.2	0.32	0.03	0.01
Gamma 0.5	0.32	0.03	0.01
Gamma 0.8	0.30	0.03	0.01

with increased aerosol scattering. Unlike γ , which is relatively constant with the fit parameter value, the κ uncertainty increases with κ . The standard deviation in γ has a strong dependence on the aerosol scattering coefficient, highlighting the difficulty in fitting a power law function to noisy data.

Table 2 shows the calculated wet scattering values normalized to a reference scattering RH of 40% and the associated uncertainties calculated from equation (3). The reported values are segregated by σ_d (1, 10, and 100), %RH (45, 60, and 85), γ (0.2, 0.5, and 0.8), and κ (0.05, 0.2, and 0.4). In general, the calculated uncertainties increase with %RH, κ and γ , and σ_d . The relative percent uncertainty decreases with increases in σ_d . The contribution from uncertainty in σ_d dominates the total uncertainty for most RH and gamma values. An exception is for $\sigma_d = 100 \text{ Mm}^{-1}$ and at 85% RH, when the error in the wet RH value contributes more to the total measurement uncertainty. The kappa uncertainty values are slightly higher than those for gamma at high fit parameter and RH values.

The high uncertainty, particularly at low scattering coefficients, highlights the difficulty in interpreting these measurements, under clean conditions such as those in polar, marine, or high-altitude locations. In these cases analysis of the long-term trends and variances of hygroscopic growth with other aerosol properties may be a more reliable predictor of aerosol scattering increase with RH. The uncertainties listed in Table 2 set lower and upper limits of hygroscopic growth estimates for remote-sensing retrievals and model simulations. The multiple RH values, aerosol loadings, and fit parameters help place boundaries on these estimates for a variety of conditions.

Table 2. Wet Scattering Coefficients, and Standard and Percent Errors in the Wet Scattering Coefficient as a Function of RH and Normalized to a Dry Scattering Coefficient (σ_d , RH = 40%) for Gamma and Kappa Fit Algorithms

σ_d	Fit parameter	Wet Scattering (Mm^{-1})			Absolute Error (Mm^{-1})			Percent Error			
		45% RH	60% RH	85% RH	45% RH	60% RH	85% RH	45% RH	60% RH	85% RH	
$\sigma_d = 1$	Gamma	45% RH	60% RH	85% RH	45% RH	60% RH	85% RH	45% RH	60% RH	85% RH	
		0.2	1.0	1.1	1.3	1.4	1.4	1.8	133.0	133.6	140.3
		0.5	1.0	1.2	2.0	1.4	1.6	2.8	133.1	133.7	140.6
	0.8	1.1	1.4	3.0	1.4	1.9	4.3	133.1	133.8	141.1	
	Kappa	45% RH	60% RH	85% RH	45% RH	60% RH	85% RH	45% RH	60% RH	85% RH	
		0.05	1.0	1.0	1.2	1.4	1.4	1.7	137.4	137.3	136.6
		0.2	1.0	1.2	2.0	1.6	1.7	2.8	150.2	148.2	142.5
	0.4	1.1	1.3	3.0	1.8	2.1	4.4	166.5	157.7	145.9	
	$\sigma_d = 10$	Gamma	45% RH	60% RH	85% RH	45% RH	60% RH	85% RH	45% RH	60% RH	85% RH
0.2			10.2	10.8	13.2	2.0	2.1	2.6	19.2	19.3	20.1
0.5			10.4	12.2	20.0	2.0	2.4	4.4	19.4	19.6	22.0
0.8		10.7	13.8	30.3	2.1	2.8	7.7	19.7	20.2	25.3	
Kappa		45% RH	60% RH	85% RH	45% RH	60% RH	85% RH	45% RH	60% RH	85% RH	
		0.05	10.1	10.4	12.5	2.0	2.1	2.6	19.9	19.9	20.9
		0.2	10.3	11.7	20.0	2.2	2.5	4.9	21.8	21.7	24.6
0.4		10.6	13.3	30.0	2.6	3.2	8.2	24.3	23.7	27.5	
$\sigma_d = 100$		Gamma	45% RH	60% RH	85% RH	45% RH	60% RH	85% RH	45% RH	60% RH	85% RH
	0.2		101.8	108.4	132.0	9.8	10.5	13.8	9.6	9.7	10.5
	0.5		104.4	122.5	200.0	10.4	12.6	27.8	10.0	10.3	13.9
	0.8	107.2	138.3	303.1	11.3	15.6	56.7	10.5	11.3	18.7	
	Kappa	45% RH	60% RH	85% RH	45% RH	60% RH	85% RH	45% RH	60% RH	85% RH	
		0.05	100.8	104.2	125.0	10.0	10.3	14.0	9.9	9.9	11.2
		0.2	103.0	116.7	200.0	11.3	13.0	33.6	11.0	11.1	16.8
	0.4	106.1	133.3	300.0	13.3	17.1	61.9	12.6	12.8	20.6	

Table 3. Mean (Standard Deviation) Aerosol Hygroscopic Growth Parameters, fRH, and Gamma (γ) and Kappa (κ) Fit Parameters for Sub-1 μm and Sub-10 μm Aerosol Size Cuts With Season^a

Parameter	Spring (MAM)	Summer (JJA)	Fall (SON)	Winter (DJF)	Annual
fRH (γ) sub-1 μm	1.91 (0.46)	1.74 (0.30)	1.85 (0.42)	1.96 (0.41)	1.87 (0.41)
fRH (γ) sub-10 μm	1.80 (0.39)	1.65 (0.27)	1.72 (0.38)	1.82 (0.37)	1.78 (0.36)
γ sub-1 μm	0.45 (0.16)	0.39 (0.12)	0.42 (0.16)	0.47 (0.16)	0.44 (0.16)
γ sub-10 μm	0.41 (0.15)	0.35 (0.12)	0.37 (0.16)	0.42 (0.15)	0.40 (0.15)
fRH (κ) sub-1 μm	2.15 (0.45)	2.01(0.33)	2.10 (0.46)	2.32 (0.46)	2.14 (0.44)
fRH (κ) sub-10 μm	2.02 (0.44)	1.86 (0.32)	1.92 (0.44)	2.16 (0.47)	1.99 (0.44)
κ sub-1 μm	0.24 (0.10)	0.20 (0.07)	0.21 (0.10)	0.26 (0.09)	0.23 (0.10)
κ sub-10 μm	0.21 (0.09)	0.17(0.06)	0.18 (0.09)	0.24 (0.09)	0.20 (0.09)

^aMAM, March–May; JJA, June–August; SON, September–November; DJF, December–February.

Our uncertainty analysis and normalizations do not account for measurement-specific conditions. Aerosol transmission loss in the humidifier will decrease the kappa fit value linearly such that a 5% aerosol loss will result in a 5% measured decrease in κ and b . This adjustment needs to be applied uniquely to each measurement system. Linear offsets to the wet scattering coefficient from aerosol losses do not affect the γ fit value. RH gradients or an ill-defined RH inside the nephelometer measurement cavity will add uncertainty. The magnitude of this bias under varying measurement conditions is under investigation.

4. Results

4.1. Temporal Variability and Aerosol Composition

Table 3 reports statistics on the sub-10 μm and sub-1 μm hygroscopic growth parameters with season. The kappa fRH values are 12–18% higher than the gamma values. The higher kappa fRH values may reflect the higher curvature of this algorithm compared to the power law gamma fit. Average fRH sigma fit values, defined as the standard deviation of the residuals, of the two fits are both 0.05 for sub-10 μm aerosol data at 550 nm. The mean standard deviation of the sigma goodness of fit value is 0.03 for both the gamma and kappa fits. For comparison the mean r^2 value for the kappa least squares fit is 0.82 ± 0.21 . The goodness of fit parameters improve with increasing scattering coefficients and hence decreased nephelometer noise to a mean sigma value of 0.02 (gamma and kappa fits) and a mean r^2 value of 0.98 (kappa fit) for scattering coefficients greater than 100 Mm^{-1} .

The ability of these two equations to characterize ambient aerosol scattering coefficients rests with the goodness of fit parameters and the RH range. The two fits diverge at high and low RH values as the kappa fit has a higher curvature than the gamma fit. Neither fit is expected to perform well at low RH values where the hygroscopic growth curves flatten. The fit quality declines at RH values $>90\%$ where the rate of hygroscopic growth increases rapidly as the aerosol approaches the transition region between subsaturated and supersaturated RH regimes. Noise and uncertainty in both RH and nephelometer scattering measurements limit fit quality with exceptionally steep hygroscopic growth rates.

As there is little difference between the seasonal trends and variances between the kappa and gamma algorithms, we only show data associated with the gamma fits in the figures. The monthly variabilities in both aerosol size ranges in Figure 1 and Table 3 show slightly lower values during the summer months. Sub-1 μm fRH values are $\sim 7\%$ higher than sub-10 μm values. This small difference reflects the presence of super- μm dust aerosol prevalent at the site. The difference in fRH between the two size cuts varies between 0.16 in October and 0.05 in August. The higher offset between the two values in the fall and early winter coincides with winter wheat planting and low precipitation. Section 4.2 offers a more detailed discussion on size-dependent hygroscopic growth behavior.

Sherman et al. [2015] note that transport to the site varies seasonally with winds predominately from the south during the summer, a region that includes Oklahoma City. Figure 2 shows wind rose plots of the fRH values with season. During winter there is a higher frequency of winds from the N-NW than other seasons: the direction of Wichita, KS, and a large agricultural region. Winds from the S-SE are more prevalent from spring to fall. Note that fRH values vary little with wind sector for any given season.

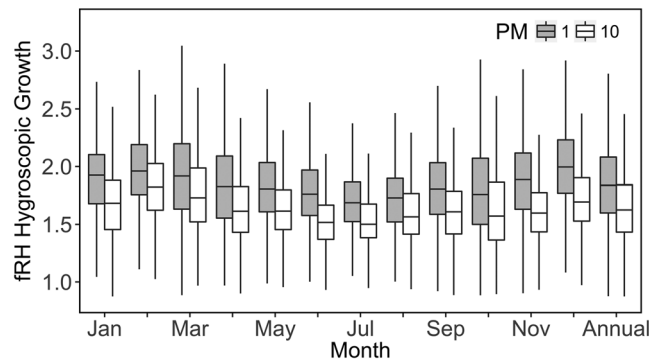


Figure 1. The box and whisker plot showing the 5, 25, 50, 75, and 95th percentiles of the sub- μm and sub- $10\ \mu\text{m}$ aerosol fRH using the gamma fit at SGP from 2009 to 2015.

frh values are highest in winter and correlate well with the nitrate ion mass concentration. The NMF (nitrate mass fraction) is highest in the cold winter and spring months when the nitrate vapor pressure is low and soil denitrification is high, particularly of unplanted fields or those fertilized in the fall [Paul and Zebarth, 1997]. During winter, a shallow inversion layer and low wind speeds keep aerosol and other pollutants near the surface, resulting in a higher aerosol loading than other seasons [Sherman et al., 2015]. While the SO_4^{2-} mass concentration has little seasonal variability, the SMF (sulfate mass fraction) is higher in summer when the NMF is low. The summer months have the lowest fRH values and also the highest aerosol organic mass fraction (OMF) [Parworth et al., 2015].

Past studies found a strong correlation between fRH and the OMF that varies with aerosol type [Quinn et al., 2005; Beyersdorf et al., 2016]. Figure 3 shows the correlation between γ and the organic mass fraction (OMF) of the nonrefractive aerosol mass measured with an aerosol mass spectrometer from 2012 to 2014 at SGP. Data are colored by the mass fraction of nitrate and sulfate ions. Three distinct modes of aerosol hygroscopic growth behavior with OMF are apparent: (1) a low rate of increase in γ with declining OMF when the nitrate mass fraction (NMF) is high and the OMF is low, (2) a higher rate of increase in γ with declining OMF in when the sulfate mass fraction (SMF) is high, and (3) a large range of γ values when the OMF is high and the NMF and SMF are both low. The linear fits for these three variances of γ versus OMF with NMF range from -0.36 at high NMF to -0.66 for when the NMF and SMF are <0.2 . We intentionally limit the gamma range of the plot to reduce the contribution of outliers that may represent smoke at low gamma or fresh sulfate aerosol formation at high gamma. As the NMF is highest in winter and spring and the SMF is higher in summer, the γ behavior with respect to the OMF varies seasonally. Similar measurements of γ versus OMF report slopes of -0.3 to -0.5 in polluted regions and -0.7 in a marine environment [Quinn et al., 2005, Massoli et al., 2009, and Beyersdorf et al., 2016].

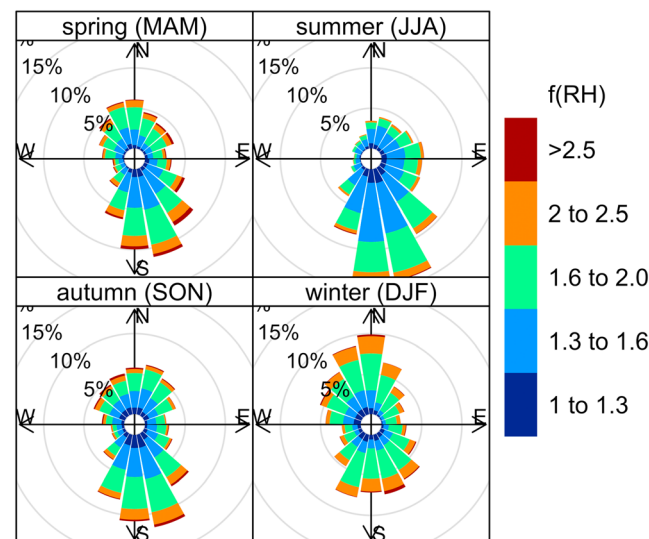


Figure 2. Seasonal wind rose plots depicting seasonal fRH values with wind direction.

4.2. Variance of fRH With Aerosol Composition

The seasonal variation in fRH is reflected in changes in the hydrophilic, inorganic composition of the PM1 aerosol. On average, organics, sulfate, nitrate, and ammonium comprise over 98% of the nonrefractive aerosol mass, with equivalent ratios of NH_4^+ to SO_4^{2-} plus NO_3^- near 1, indicating a mostly neutral aerosol [Parworth et al., 2015].

fRH values are highest in winter and correlate well with the nitrate ion mass concentration. The NMF (nitrate mass fraction) is highest in the cold winter and spring months when the nitrate vapor pressure is low and soil denitrification is high, particularly of unplanted fields or those fertilized in the fall [Paul and Zebarth, 1997]. During winter, a shallow inversion layer and low wind speeds keep aerosol and other pollutants near the surface, resulting in a higher aerosol loading than other seasons [Sherman et al., 2015]. While the SO_4^{2-} mass concentration has little seasonal variability, the SMF (sulfate mass fraction) is higher in summer when the NMF is low. The summer months have the lowest fRH values and also the highest aerosol organic mass fraction (OMF) [Parworth et al., 2015].

A remarkable feature of Figure 3 is the wide range of γ values for $\text{OMF} > 0.7$. Using Positive Matrix Factorization, Parworth et al. [2015] categorized the organic aerosol mass composition into more or less oxidized and biomass burning components. Variation in the relative mass fractions of these organic components between seasons likely contributed to the variability in γ at high OMF. Not enough data were available to compare γ to the level of organic aerosol oxidation. Smoke aerosol, particularly aged smoke from long-range transport, could be a factor in the large variance of gamma at high aerosol OMF. Jing

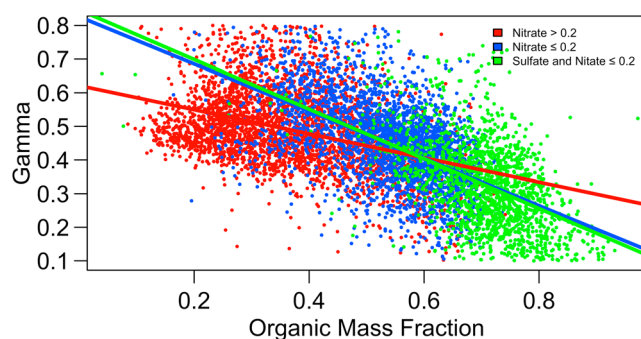


Figure 3. Variation of the gamma fit parameter with aerosol organic mass fraction and colored by nitrate and sulfate mass fraction amounts. The red and blue fit lines correspond to data with similar color. The green fit line is for the entire data set.

with the OMF. Figure 4 highlights this correlation and shows the size-dependent, aerosol hygroscopic growth with respect to the organic mass content. Larger aerosols with lower backscatter fractions (BSF) are confined to lower OMF and higher γ values. The high nitrate and sulfate mass fractions of this larger, more hygroscopic aerosol may reflect an aged aerosol that has undergone secondary gas and aqueous phase oxidation processes. Smaller aerosol with higher backscatter fractions were concentrated at OMF values higher than 0.5 and exhibited a high range of γ values from 0.1 to about 0.6. Typically, smaller aerosols represent fresh emissions with a high organic content. Figure 4 shows a more varied small particle composition. The broad range of small particle hygroscopic growth at OMF > 0.5 may reflect variability in the organic aerosol oxidation state with more oxidized organics at higher γ values or, as already discussed, the presence of inorganic potassium salts in smoke aerosol.

4.3. Systematic Variability With Aerosol Optical Properties

Figure 5 shows the fRH variance with the intensive aerosol optical properties: scattering and absorption Ångström coefficients, backscatter fraction, and single scattering albedo. The solid black lines show the systematic relationships between the aerosol optical properties and aerosol hygroscopicity. Both the aerosol single scatter albedo (SSA) and absorption Ångström exponent (AAE) are measures of aerosol elemental (EC) and organic brown (OC) carbon absorption. The mass absorption efficiency of OC increases at shorter visible wavelengths, resulting in higher AAE values [Barnard *et al.*, 2008]. Because nonabsorbing aerosol coatings can enhance this wavelength dependence [Lack and Cappa, 2010], AAE is only a rough proxy of the organic aerosol content. SSA represents the relative aerosol scattering to extinction such that lower values indicate a stronger absorption and thus higher OC and EC content. Sherman *et al.* [2015] show that the AAE declines with increasing SSA, indicating a lower contribution of OC relative to EC at high SSA. As shown in Figures 5a and 5b, fRH increases with decreasing AAE (brown carbon) and increasing SSA (lower total carbon absorption). The correlation of fRH to aerosol AAE and SSA affirms the relationship with the ACSM chemistry data in Figure 3 of a declining aerosol hygroscopic growth with increasing organic mass fraction. The probability distribution of points (dotted lines) show an AAE peak probability at ~1.45, indicating a moderate influence of absorbing organics. The SSA peak

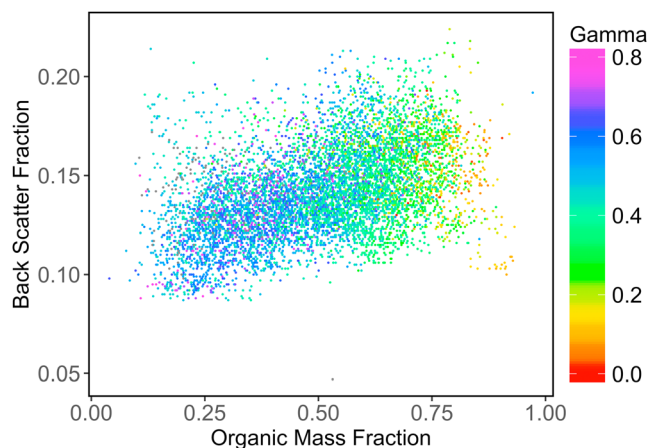


Figure 4. Sub-1 μm aerosol backscattering fraction at 550 nm versus organic mass fraction from ACSM.

et al. [2017] report that potassium salts prevalent in smoke aerosol make a significant contribution to organic aerosol hygroscopic growth. A known controlled burn of an adjacent field to SGP on 17 July 2015 had aerosol gamma values of 0.2 and 0.3 over the two 1 h episodes, corresponding to fRH values of 1.32 and 1.5, respectively. For this particular event, fresh smoke aerosol likely had a high enough inorganic composition to significantly influence the aerosol hygroscopicity.

Aerosol size also plays a role in the scattering hygroscopic growth variance

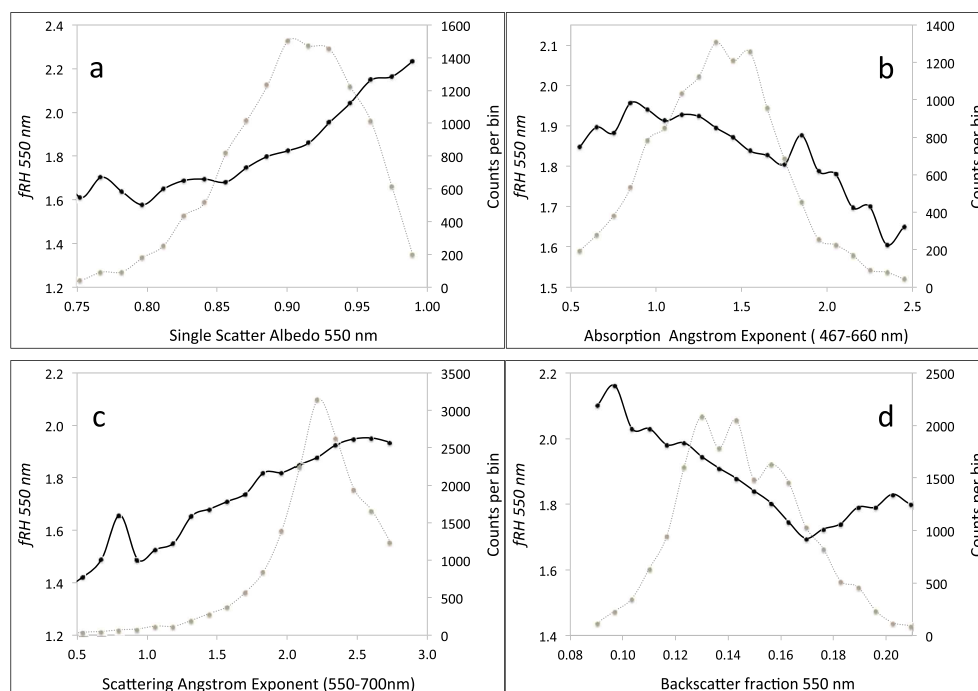


Figure 5. Plots of binned fRH versus dry, intensive, aerosol optical properties (solid line), and the probability distributions of the intensive properties (gray line). Intensive properties are (a) single scatter albedo at 550 nm, (b) absorption Ångström exponent for the 467:530 nm wavelength pairs, (c) scattering Ångström exponent for the 450:700 nm wavelength pairs, and (d) the backscatter fraction at 550 nm.

probability at 0.93 and relatively narrow range of values indicate the presence of a highly scattering aerosol at SGP with a moderate to low concentration of absorbing carbon.

Normally, aerosol EC absorption is constant across the visible spectrum with an AAE of ~ 1 . However, aerosol coatings that form an outer shell around a dark EC core can preferentially focus certain wavelengths by acting as a waveguide, an effect known as “lensing.” *Lack and Cappa* [2010] predict values of AAE < 1 in their model of clear coatings on an EC core for aerosol in the larger end of the accumulation mode with particles diameters > 150 nm. Here low values of AAE < 1 at SGP are associated with high SSA values as well as larger accumulation mode particles with low BSF and low OMF values. As shown in Figure 5b, AAE < 1 have a relatively high hygroscopicity with fRH values of ~ 1.9 . The low AAE values possibly indicate an absorption enhancement of longer wavelengths due to a clear aerosol coating. However, the lensing effect is difficult to separate from filter artifacts, making the underlying reason for AAE < 1 values unclear. Measurements of aerosol gas phase absorption could give further insight on the role of coatings and aerosol absorption.

The aerosol scattering Ångström exponent and backscatter fraction are two optical properties that decrease with increasing aerosol size. These two parameters often anticorrelate, particularly if the aerosol has a bimodal distribution [*Schuster et al.*, 2006]. Figures 5c and 5d show plots of the hygroscopic growth parameter increasing with the scattering Ångström exponent (SAE) and decreasing with the backscatter fraction (BSF). Here fRH exhibits differing size-dependent behavior with SAE and BSF at SGP. These size-dependent aerosol parameters represent different regions of the aerosol accumulation mode. The BSF is sensitive to size changes of smaller diameter particles, whereas SAE for the given wavelength pair (550 nm/700 nm) is more representative of the upper size range of the aerosol accumulation mode and the super- μm , coarse mode. A previous study of the hygroscopic diameter growth, gRH, found the aerosol water uptake at SGP increased with aerosol size up to $0.3 \mu\text{m}$ and then decreased for larger particles [*Gasparini et al.*, 2006b]. The $0.3 \mu\text{m}$ diameter peak in gRH and decline at larger diameters reflects the changing composition and hygroscopic growth of two modes in a bimodal aerosol size distribution. This bimodal behavior shows up in the differing size-dependent, hygroscopic growth behavior of the BSF and SAE parameters.

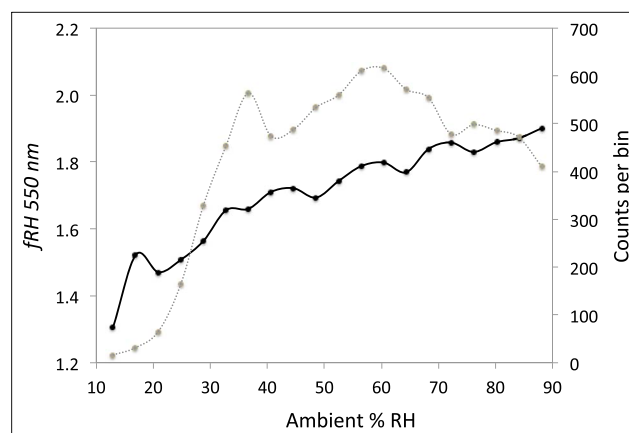


Figure 6. fRH (85%/40%) for sub-10 μm data binned by the ambient RH (solid line) and the binned probability distribution of the ambient RH (dashed line).

4.4. Variance of Hygroscopic Growth With Ambient Relative Humidity

The ambient RH affects the aqueous phase chemistry within aerosols, the particle viscosity, and also the gas to aerosol partitioning of chemical species, three factors that influence aerosol hygroscopic growth. At SGP, the median ambient relative humidity over the measurement period was 63% with a lower 25th quartile of 45% and an upper 75th quartile of 79%. Though the ambient RH has a pronounced diurnal cycle, it exhibits little seasonal variation. Figure 6 shows the dependence of fRH for sub-10 μm aerosol at 550 nm on the ambient RH. On average, fRH for sub-10 μm aerosol increases from about

1.4 to about 1.9 as the ambient RH increased from 40 to 80%. The dotted line of the fRH distribution with RH shows that most of the measurements occur when the ambient RH is between 20 and 80%.

The aerosol chemistry responsible for RH dependence of hygroscopic growth is ambiguous. The aerosol mass fractions of inorganic species exhibit little correlation with the ambient RH, while the OMF slightly declines with an increase in ambient RH. In contrast, the mass loadings of nitrate, sulfate, and ammonium increased with ambient RH in accordance with the reduced vapor pressure with increasing RH of gas phase ammonia, sulphuric and nitric acid [Marti *et al.*, 1997; Stelson and Seinfeld, 1982]. Because of their weak RH dependence, the relative mass fractions of the total inorganic and organic species cannot account for the fRH increase with ambient RH. Instead, the increase in fRH with ambient RH may reflect the organic component oxidation level. Better aerosol chemical data with resolved organic oxidation level would help discern the reason for the positive correlation between fRH and the ambient RH.

In addition to heterogeneous oxidation of gas phase species, in-cloud oxidation will enhance the aerosol sulfate, nitrate, and oxidized organic mass fractions. Low-level cloud coverage and cloud probability increase with the ambient RH at SGP with the highest cloud probability at RH values between 75 and 85% [Kennedy *et al.*, 2010]. In-cloud oxidation may contribute to not only the increase in fRH with RH but also the prevalence of bimodal aerosol size distributions at SGP [Gasparini *et al.*, 2006b].

4.5. Instrument RH and Aerosol Phase Change

The lowest instrument RH prior to hydration will affect the aerosol phase, whether it remains liquid, becomes more viscous or solid. For a mostly inorganic aerosol, the RH scattering growth behavior will move to the lower branch of the hysteresis curve if the instrument RH drops below the efflorescence RH. The lowest RH in the system prior to humidification is in the internal dry nephelometer which ranges from 5 to 60% RH for the hydration curves that meet the fit criteria. The internal instrument RH varies with the ambient dew point. Dew point values at SGP vary from as low as -20°C in the winter to values as high as 26°C in the summer. Over the summer when high dew points are prevalent, SGP aerosol consists of mostly low-volatility, highly oxidized organic species [Parworth *et al.*, 2015]. As such, the summer aerosol is likely invariant to changes in the sampling RH for an instrument RH above $\sim 30\%$. However, during the cold winter months, the sampling RH can drop below the efflorescence RH of most inorganic salts. Figure 7 shows a graph of binned fRH and SMF versus the dry nephelometer RH. Note that 98% of the data that met the fit conditions were when the dry nephelometer % RH is $< 50\%$. The dry nephelometer RH tracks the ambient dew point with low values in the winter and increasing RH through spring and summer. Both fRH and the SMF increase at dry nephelometer RH values greater than 50%. These times are infrequent but are typical of high dew points during the summer daytime. The increase in fRH at high sampling RH possibly indicates a phase transition but may also reflect daytime photochemical production of aerosol sulfate and oxidized organics. A lower fit quality with decreasing instrument RH is expected if the growth behavior does not fit the

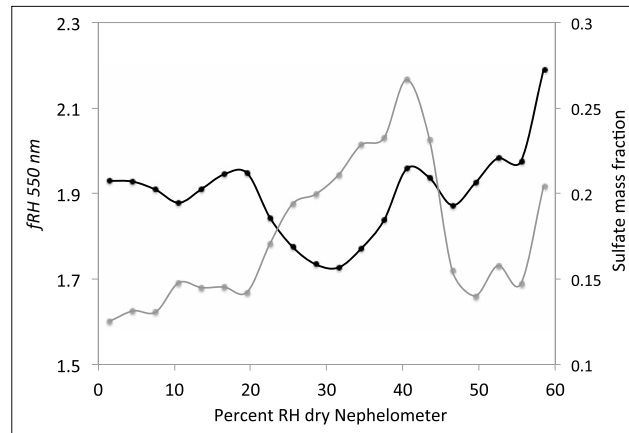


Figure 7. fRH (solid line) and the SMF (gray line) binned by the dry nephelometer RH.

behavior, their finding denotes an externally mixed aerosol in these air samples. In another study, closure measurements of nephelometer fRH with aerosol diameter hygroscopic growth, gRH, at SGP [Gasparini et al., 2006a] indicated that the sampled nephelometer aerosol was more frequently metastable than crystalline. A step change in aerosol scattering with RH is difficult to observe over a broad size range of scattering

expected algorithms of a metastable aerosol. However, trend analysis did not show a correlation between the dry nephelometer RH and of the fRH sigma goodness of fit parameters.

Looking at deliquescence with size-dependent hygroscopic growth, Martin et al. [2008] measured the aerosol phase activity with RH of 150 nm particles at SGP. They found deliquescence in 13% of their humidifier scans. Approximately ~30% of the 150 nm particles in these 13 scans exhibit a phase change at ~80% RH, similar to that of $(\text{NH}_4)_2\text{SO}_4$. With only a fraction of the particles exhibiting deliquescent behavior, their finding denotes an externally mixed aerosol in these air samples. In another study, closure measurements of nephelometer fRH with aerosol diameter hygroscopic growth, gRH, at SGP [Gasparini et al., 2006a] indicated that the sampled nephelometer aerosol was more frequently metastable than crystalline. A step change in aerosol scattering with RH is difficult to observe over a broad size range of scattering measurements, especially if the aerosol is externally mixed with a lesser fraction being deliquescent.

While difficult to discern with broad statistics, case-by-case analysis of phase changes is observed. Figure 8 shows an example of how aerosol phase impacts fit quality. The figure shows the aerosol hygroscopic growth profiles before, during, and after a large change in wind direction and source emissions at SGP on 10 April 2011. Over the course of 3 h the aerosol scattering coefficients decline by ~60% and the ambient RH dropped from 80 to 20% (dew point drop of 16°C). Figure 8b shows the hourly humidifier RH scans and the ratio of wet:dry scattering coefficients (fRH). The smoothly varying scan at 13:00 UTC tracks both the kappa and gamma algorithms well with little deviation of the data from the fit lines. At 14:00 the humidifier scan is uneven as the air mass changed during the hour. After the aerosol scattering coefficient stabilized, at 15:00 UTC, the scattering enhancement increased at a faster rate above an RH of 70%, causing the fit lines to overpredict growth behavior from 58 to 70% RH and underpredict the wet scattering enhancement at higher %RH values as shown in Figure 8c. The abrupt increase in the hygroscopic growth rate

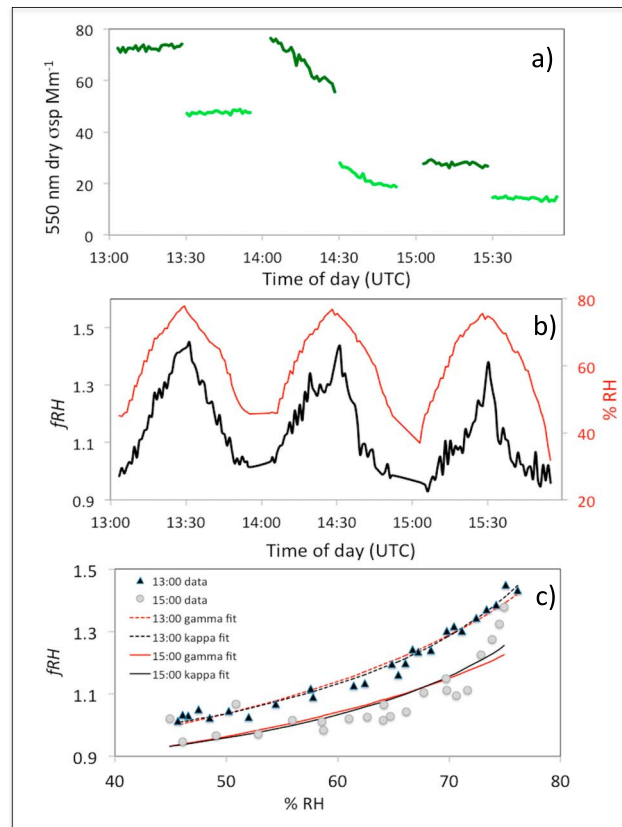


Figure 8. Plots of aerosol scattering data from 10 April 2011 at SGP showing (a) The sub-10 μm (dark green) and sub- μm (light green) scattering coefficients at 550 nm, (b) ratio of the wet/dry scattering coefficients (black) and humidifier % RH (red), and (c) plots of the fRH data fit to the gamma and kappa fit algorithms at 13:00 (black triangles) and at 15:00 (gray circles).

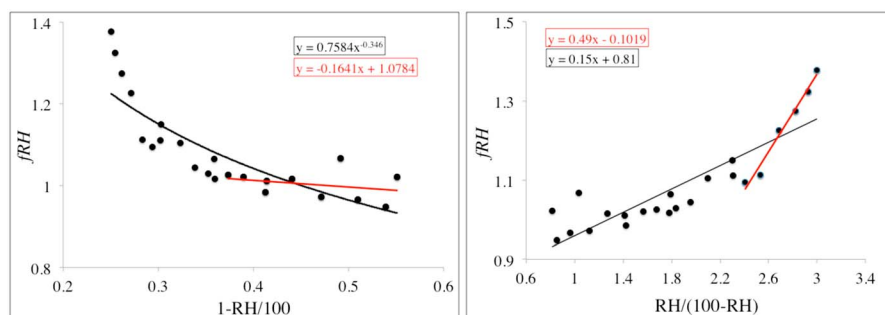


Figure 9. Plots of (left) gamma and (right) kappa hygroscopic growth fits. The red lines are linear fits of the data over a limited RH range. Data from sub- μm aerosol scattering coefficients at 550 nm on 10 April 2011 at SGP. Fit equation boxes are colored the same as the corresponding fit line.

at a high RH likely reflects a change in the aerosol phase. The deviation of the data from the fRH fit line is as much as 0.15 (40%) at 75% RH. This error increases with %RH. However, at the ambient RH of 20% of this measurement period, hygroscopic growth likely did not influence the ambient aerosol scattering coefficient.

Methods that compare changes in the hygroscopic growth rate over the RH range can help identify potential phase changes. Such an analysis necessitates a high scattering signal with low noise and so biases the data to times with high aerosol loading. Zhang *et al.* [2015] introduce a steepness parameter that evaluates changes in the fit derivative at two RH values. A more robust comparison using the gamma algorithm compares the slope of a fit line from ~ 40 to 60% RH to the power law fit parameter γ . For an ideal fit this ratio is ~ -2 . A ratio > -2 indicates a much lower slope or slower increase with RH at low RH compared to a fit of the full range of RH. A similar comparison with the kappa algorithm involves a comparison of κ_{sca} over the entire RH range to the fit slope for $RH > 65\%$. A significantly higher slope of the high RH fit line compared to that of the entire range of values likely signifies a change in aerosol phase. Figure 9 shows an example of the two fit comparisons using the same data from Figure 8 at 15:00 UTC. The RH range of each fit was optimized to exploit the changes in growth behavior with RH. In this case, the significant increase in the kappa fit slope at high RH likely stems from change in aerosol phase or viscosity. Phase change analyses using ratios over different RH ranges are nuanced and depend on the chosen RH range, goodness of fit, and fit algorithm. Size dependence of the aerosol scattering efficiency, size-dependent transmission losses, or unidentified temperature gradients can result anomalous scattering growth with RH. Further corroboration of this method with aerosol composition and size-dependent hygroscopic growth would be useful. More distinct phase transition behavior is expected at sites with higher inorganic composition. Though simple, this ratio technique works well in identifying broad trends in the aerosol phase behavior for a large data set. Rather than a binary view of the aerosol as being on an upper or lower branch of a phase hysteresis, the method allows for a continuum of phase behavior present in externally mixed aerosol.

5. Discussion

Long-term measurements probe large-scale processes that span seasons and years. Statistical analysis of these large data sets shows systematic relationships between variables over a range of conditions that then illuminate feedback between the boundary layer, hydrologic, radiation, and aerosol cycles. The covariances and trends conceptualize atmospheric aerosol dynamics in broad terms that help us intuit this forcing. Though often qualitative, the empirical relationships place boundaries on remote sensing retrievals and climate models. Although the fRH measurements presented here show distinct trends and variances, the uncertainty and possible phase transitions associated with these measurements place limits around the scope of their use. Locations with low aerosol loading or low dew point need high scrutiny. The intent of the analysis presented here is to optimize fRH data use in evaluation of remote sensing and model products.

Statistically, the two algorithms presented, kappa and gamma, had comparable fit uncertainties over the range of the entire data set. For an individual humidifier scan one fit may perform better than the other with respect to a high or low RH range or steepness of the scattering growth with RH. The gamma parameterization

performs poorly at very low RH where the growth rate flattens and at high RH values above 90% where the growth rate rapidly increases near the transition between subsaturated and supersaturated regimes [Brock *et al.*, 2016]. In general, the two algorithms fit the hygroscopic growth behavior well within the RH range of these measurements with relatively low sigma goodness of fit values (standard deviation) over a broad range of aerosol scattering values. The uncertainty calculations are for a generic hydration scan and do not account for calibration errors or other instrument-specific error outside of normal operating conditions. Such circumstances need an individual evaluation of measurement error. Signal noise from the aerosol scattering coefficients is the largest contributor to the fit error such that scattering values less than 10 Mm^{-1} may not yield reasonable values of gamma or kappa. Reduction of scattering coefficient noise can be achieved by performing hour-long scans with a 2 min average of the data. This comes with a reduction in temporal resolution and increased risk of the air mass and aerosol properties changing over the measurement period. For sites with low aerosol loading and little air mass variability the longer scan time will reduce the fit error.

Alternatively, the fit parameters can be approximated from known cross correlations with aerosol optical and/or chemical properties. As long-term aerosol scattering hygroscopic growth measurements are sparse, these cross correlations of the fit parameters with more common in situ measurements of aerosol optical properties will enhance the global coverage of aerosol fRH. Large aerosol observation networks such as the NOAA federated network (www.esrl.noaa.gov/gmd/aero); Aerosols, Clouds, and Trace gases Research Infrastructure Network (www.actris.net); and Department of Energy (DOE) ARM (www.arm.gov) provide long-term measurements of aerosol optical properties for such analysis.

Aerosol fRH at SGP has a strong seasonal variance, driven mostly by changes in the aerosol chemistry. Higher winter values are attributed to a high NMF that results from a low nitric acid vapor pressure at colder temperatures. The lower summer time fRH values accompany a higher OMF. Despite changes in the predominant transport sector with season, fRH exhibited little variation with wind sector for a given season. This suggests that local aerosol emissions and/or similar, sector-independent processes such as photochemical oxidation, cloud processing, and temperature-dependent vapor pressures, regulate the aerosol hygroscopic growth behavior for a given season. The average fRH values reported here are comparable to median values reported by Sheridan *et al.* [2001] from SGP of 1.83 (sub- $10 \mu\text{m}$) and 1.86 (sub- μm). The lower sub- $10 \mu\text{m}$ fRH values may indicate an influence from dust. For comparison, fRH measurements from other rural regions in the western U.S. report values that range from as low as 1.26 in California [Malm *et al.*, 2005] to as high as 2.06 in Texas [Malm *et al.*, 2003].

Strong correlations between the aerosol hygroscopic growth, chemistry, and optical properties indicate that these properties are closely coupled. Changes in fRH associated with optical and chemical properties suggest that larger, less absorbing, more oxidized particles with a lower OMF have a higher hygroscopic growth. This behavior is not necessarily repeated for larger particles that may include coarse mode dust, a higher organic fraction, or aerosols large enough for their scattering efficiency to decline at 550 nm with increased growth. The aerosol fRH showed opposing behavior with BSF and SAE, with increased water uptake with size for smaller accumulation mode aerosol (BSF) and decreased water uptake with size for larger accumulation and coarse mode particles (SAE). These correlations with aerosol optical and chemical properties can be used to constrain the hygroscopic fit parameter when fRH measurements are not present, the fit quality is low, or the aerosol scattering values are too low to give a reliable fit parameter. The correlations are specific to SGP but may be extended to regions with similar aerosol type and climate.

Aerosol phase spans the range of a liquid solution to a viscous, amorphous liquid to a mixed phase aerosol with solid inclusions to a solid. These phases can vary with aerosol size and between internally and externally mixed particles. Trends in the hygroscopic growth fit parameter with large differences between the dry sample and ambient RH were ambiguous and neither support nor discount sampling-induced changes in aerosol phase. Phase shift behavior, as observed from scattering hygroscopic growth measurements, is subtle for an aged, mostly organic aerosol. Distinct discontinuity in the humidification scans will not be observed unless a large enough fraction of the optically active aerosol deliquesces. We present two methods which ratio the scattering growth behavior over differing RH ranges to infer a phase change. The methods are qualitative and limit analysis to data with low noise. Unlike detailed closure measurements, this ratio method is an effective tool to evaluate long-term changes in aerosol phase under varying meteorological conditions for different aerosol types. The analysis is meant to point out potential feedback or perhaps measurement problems. A

significant deviation in these ratios may point to a change in aerosol chemistry, transport, meteorology, or measurement. As was the case for the data in Figures 8 and 9, a change in aerosol phase accommodated an abrupt change in air mass, signified by a large change in dew point and wind direction. Similar feedback in aerosol phase behavior with changes in aerosol chemistry and size, entrainment, or precipitation events would enhance understanding of the aerosol lifecycle.

Much more can be accomplished with this data set and similar data sets of the RH-dependent aerosol scattering behavior in the DOE ARM archive. Extensions of this study are to repeat the analysis for other sites and aerosols types such as marine, smoke, pollution, and forested regions and a comparison of in situ surface measurements of aerosol extinction f_{RH} with RH-dependent retrievals from remote sensing measurements. Decoupling the aerosol optical properties from the ambient RH can improve the remote sensing retrievals as well as radiative forcing model parameterizations.

Acknowledgments

The authors acknowledge support from the U.S. Department of Energy Atmospheric Radiation Measurement Program via Argonne National Laboratory, the National Oceanic and Atmospheric Administration Earth Systems Research Laboratory and the AG Foundation. The authors thank the DOE SGP ARM Climate Research Facility staff and scientists who helped maintain the instruments and ingest the data used for this paper, particularly Patrick Dowell, Ken Teske, Matt Gibson, Annette Koontz, and Connor Flynn. In situ aerosol optical measurement data are available from the DOE ARM archive at <https://www.arm.gov/data>. Algorithm and uncertainty calculations are available at ftp://aftp.cmdl.noaa.gov/user/anne/jgrd_54088.

References

- Anderson, T. L., and J. A. Ogren (1998), Determining aerosol radiative properties using the TSI 3563 integrating nephelometer, *Aerosol Sci. Technol.*, *29*, 57–69.
- Anderson, T. L., D. S. Covert, J. D. Wheeler, J. M. Harris, K. D. Perry, B. E. Trost, D. J. Jaffe, and J. A. Ogren (1999), Aerosol backscatter fraction and single-scattering albedo: Measured values and uncertainties at a coastal station in the Pacific Northwest, *J. Geophys. Res.*, *104*, 26,793–26,807, doi:10.1029/1999JD900172.
- Barnard, J. C., R. Volkamer, and E. I. Kassianov (2008), Estimation of the mass absorption cross section of the organic carbon component of aerosols in the Mexico City metropolitan area, *Atmos. Chem. Phys.*, *8*, 6665–6679, doi:10.5194/acp-8-6665-2008.
- Bar-Or, R. Z., I. Koren, O. Altaratz, and E. Fredj (2012), Radiative properties of humidified aerosols in a cloudy environment, *Atmos. Res.*, *118*, 280–294, doi:10.1016/j.atmosres.2012.07.014.
- Beyersdorf, A. J., L. D. Ziemba, G. Chen, C. A. Corr, J. H. Crawford, G. S. Diskin, R. H. Moore, K. L. Thornhill, E. L. Winstead, and B. E. Anderson (2016), The impact of aerosol loading, composition, and water uptake on aerosol extinction variability in the Baltimore-Washington, D. C. region, *Atmos. Chem. Phys.*, *16*, 1003–1015, doi:10.5194/acp-16-1003-2016.
- Bond, T. C., T. L. Anderson, and D. Campbell (1999), Calibration and inter-comparison of filter-based measurements of visible light absorption by aerosols, *Aerosol Sci. Technol.*, *30*, 582–600, doi:10.1080/027868299304435.
- Brock, C. A., et al. (2016), Aerosol optical properties in the southeastern United States in summer—Part 1: Hygroscopic growth, *Atmos. Chem. Phys.*, *16*, 4987–5007, doi:10.5194/acp-16-4987-2016.
- Carricío, C. M., M. D. Petters, S. M. Kreidenweiss, J. L. Colett, G. Engling, and W. C. Malm (2008), Aerosol hygroscopicity and cloud droplet activation of extracts of filters from biomass burning experiments, *J. Geophys. Res.*, *113*, D08206, doi:10.1029/2007JD009274.
- Covert, D. S., R. J. Charlson, and N. C. Ahlquist (1972), A study of the relationship of chemical composition and humidity to light scattering by aerosols, *J. Appl. Meteorol.*, *11*, 968–976.
- Engelhart, G. J., L. Hildebrandt, E. Kostenidou, N. Mihalopoulos, N. M. Donahue, and S. N. Pandis (2011), Water content of aged aerosol, *Atmos. Chem. Phys.*, *11*, 911–920, doi:10.5194/acp-11-911-2011.
- Fierz-Schmidhauser, R., P. Zieger, G. Wehrle, A. Jefferson, J. A. Ogren, U. Baltensperger, and E. Weingartner (2010), Measurement of relative humidity dependent, light scattering of aerosols, *Atmos. Meas. Tech. Discuss.*, *3*, 39–50.
- Gasparini, R., D. R. Collins, E. Andrews, P. J. Sheridan, J. A. Ogren, and J. G. Hudson (2006a), Coupling aerosol size distributions and size-resolved hygroscopicity to predict humidity-dependent optical properties and cloud condensation nuclei spectra, *J. Geophys. Res.*, *111*, D05S13, doi:10.1029/2005JD006092.
- Gasparini, R., R. Li, D. R. Collins, R. A. Ferrare, and V. G. Brackett (2006b), Application of aerosol hygroscopicity measured at the Atmospheric Radiation Measurement Program's Southern Great Plains site to examine composition and evolution, *J. Geophys. Res.*, *111*, D05S12, doi:10.1029/2004JD005448.
- Gasso, S., et al. (2000), Influence of humidity on the aerosol scattering coefficient and its effect on the upwelling radiance during ACE-2, *Tellus*, *52B*, 546–567.
- Gund, G., F. Wien, and W. F. Weisweiler (1991), Oxidation of SO₂ to sulfate in sea salt aerosols, *J. Anal. Chem.*, *340*, 616, doi:10.1007/BF00321522.
- Heintzenberg, J., et al. (2006), Intercomparisons and aerosol calibrations of 12 commercial integrating nephelometers of three manufacturers, *J. Atmos. Oceanic Tech.*, *23*, 902–914.
- Jefferson, A. (2010), Empirical estimates of CCN from aerosol optical properties at four remote sites, *Atmos. Chem. Phys.*, *10*(14), 6855–6861, doi:10.5194/acp-10-6855-2010.
- Jing, B., C. Peng, Y. Wang, Q. Liu, S. Tong, Y. Zhang, and M. Ge (2017), Hygroscopic properties of potassium chloride and its internal mixtures with organic compounds relevant to biomass burning aerosol particles, *Nature*, doi:10.1038/srep43572.
- Kasten, F. (1969), Visibility forecast in the phase of pre-condensation, *Beitr. Phys. Atmos.*, *41*, 631–635.
- Kuang, Y., C. S. Zhao, J. C. Tao, Y. X. Bian, N. Ma, and G. Zhao (2017), A novel method to derive the aerosol hygroscopicity parameter based only on measurements from a humidified nephelometer system, *Atmos. Chem. Phys.*, doi:10.5194/acp-2016-1066.
- Kennedy, A. D., X. Q. Dong, B. K. Xi, P. Minnis, A. D. Del Genio, A. B. Wolf, and M. M. Khaiyer (2010), Evaluation of the NASA GISS single-column model simulated clouds using combined surface and satellite observations, *J. Clim.*, *23*, 5175–5192, doi:10.1175/2010JCLI3353.1.
- Kinne, S., et al. (2006), An AeroCom initial assessment—Optical properties in aerosol component modules of global models, *Atmos. Chem. Phys.*, *6*, 1815–1834.
- Kotchenruther, R. A., P. V. Hobbs, and D. A. Hegg (1999), Humidification factors for atmospheric aerosols off the mid-Atlantic coast of the United States, *J. Geophys. Res.*, *104*, 2239–2251, doi:10.1029/98JD01751.
- Lack, D. A., and C. D. Cappa (2010), Impact of brown and clear carbon on light absorption enhancement, single scatter albedo and absorption wavelength dependence of black carbon, *Atmos. Chem. Phys.*, *10*, 207–4220, doi:10.5194/acp-10-4207-2010.
- Lewandowski, M., M. Jaoui, J. H. Offenberg, J. D. Krug, and T. E. Kleindienst (2015), Atmospheric oxidation of isoprene and 1,3-butadiene: Influence of aerosol acidity and relative humidity on secondary organic aerosol, *Atmos. Chem. Phys.*, *15*, 3773–3783, doi:10.5194/acp-15-3773-2015.

- Lewis, E. R., and S. E. Schwartz (2004), *Sea Salt Aerosol Production: Mechanisms, Methods, Measurements, and Models*, AGU, Washington, D. C. Section 2.5.3
- Malm, W. C., D. E. Day, S. M. Kreidenweis, J. L. Collet, and T. Lee, (2003). Humidity-dependent optical properties of fine particles during the Big Bend regional aerosol and visibility observational study. *J. Geophys. Res.*, *108*(D9), 4279, doi:10.1029/2002JD002998.
- Malm, W. C., D. E. Day, S. M. Kreidenweis, J. L. Collett Jr., C. M. Carrico, G. McMeeking, and T. Lee (2005), Hygroscopic properties of an organic-laden aerosol, *Atmos. Environ.*, *39*, 4969e4982.
- Marti, J. J., R. J. Weber, P. H. McMurry, F. L. Eisele, D. J. Tanner, and A. Jefferson (1997), New particle formation at a remote continental site: Assessing the contributions of SO₂ and organic precursors, *J. Geophys. Res.*, *102*, 6331–6339, doi:10.1029/96JD02545.
- Martin, S. T., T. Rosenoem, Q. Chen, and D. R. Collins (2008), Phase changes of ambient particles in the Southern Great Plains of Oklahoma, *Geophys. Res. Lett.*, *35*, L22801, doi:10.1029/2008GL035650.
- Massoli, P., T. S. Bates, P. K. Quinn, D. A. Lack, T. Baynard, B. M. Lerner, S. C. Tucker, J. Brioude, A. Stohl, and E. J. Williams (2009), Aerosol optical and hygroscopic properties during TexAQS-GoMACCS 2006 and their impact on aerosol direct radiative forcing, *J. Geophys. Res.*, *114*, D00F07, doi:10.1029/2008JD011604.
- Nguyen, T. K. V., Q. Zhang, J. L. Jimenez, M. Pike, and A. M. Carlton (2016), Liquid water: Ubiquitous contributor to aerosol mass, *Environ. Sci. Technol. Lett.*, *3*, 257–263, doi:10.1021/acs.estlett.6b00167.
- Ogren, J. A. (2010), Comment on "Calibration and Intercomparison of filter-based measurements of visible light absorption by aerosols", *Aerosol Sci. Technol.*, *44*, 589–591, doi:10.1080/02786826.2010.482111.
- Parworth, C., J. Fast, F. Mei, T. Shippert, C. Sivaraman, A. Tilp, T. Watson, and Q. Zhang (2015), Long-term measurements of submicrometer aerosol chemistry at the Southern Great Plains (SGP) using an Aerosol Chemical Speciation Monitor (ACSM), *Atmos. Environ.*, *106*, 43–55, doi:10.1016/j.atmosenv.2015.01.060.
- Paul, J. W., and B. J. Zebarth (1997), Denitrification and nitrate leaching during the fall and winter following cattle slurry application, *Can. J. Soil Sci.*, *77*, 231–240.
- Petters, M. D., and S. M. Kreidenweis (2007), A single parameter representation of hygroscopic growth and cloud condensation nucleus activity, *Atmos. Chem. Phys.*, *7*, 1961–1971, doi:10.5194/acp-7-1961-2007.
- Pueschel, R. F., R. J. Charlson, and N. C. Ahlquist (1969), On the anomalous deliquescence sea-spray aerosols, *J. Appl. Meteorol.*, *11*, 995–998.
- Quinn, P. K., et al. (2005), Impact of particulate organic matter on the relative humidity dependence of light scattering: A simplified parameterization, *Geophys. Res. Lett.*, *32*, L22809, doi:10.1029/2005GL024322.
- Randles, C. A., L. M. Russell, and V. Ramaswamy (2004), Hygroscopic and optical properties of organic sea salt aerosol and consequences for climate forcing, *Geophys. Res. Lett.*, *31*, L16108, doi:10.1029/2004GL020628.
- Saide, P. E., J. Kim, C. H. Song, M. Choi, Y. Cheng, and G. R. Carmichael (2014), Assimilation of next generation geostationary aerosol optical depth retrievals to improve air quality simulations, *Geophys. Res. Lett.*, *41*, 9188–9196, doi:10.1002/2014GL02089.
- Schuster, G. L., O. Dubovik, and B. N. Holben (2006), Angstrom exponent and bimodal aerosol size distributions, *J. Geophys. Res.*, *111*, D07207, doi:10.1029/2005JD006328.
- Sheridan, P. J., D. J. Delene, and J. A. Ogren (2001), Four years of continuous surface aerosol measurements from the Department of Energy's atmospheric measurement program Sothern Great Plains cloud and radiation testbed site, *Geophys. Res. Lett.*, *106*, 20,735–20,747, doi:10.1029/2001JD000785.
- Sheridan, P. J., et al. (2005), The Reno aerosol optics study: An evaluation of aerosol absorption measurement methods, *Aer. Sci. Tech.*, *39*, 1–16, doi:10.1080/027868290901891.
- Sherman, J. P., P. J. Sheridan, J. A. Ogren, E. A. Andrews, L. Schmeisser, A. Jefferson, and S. Sharma (2015), A multi-year study of lower tropospheric aerosol variability and systematic relationships from four North American regions, *Atmos. Chem. Phys.*, *15*, 12,487–12,517, doi:10.5194/acp-15-12487-2015.
- Shinozuka, Y., et al. (2015), The relationship between cloud condensation nuclei (CCN) concentration and light extinction of dried particles: Indications of underlying aerosol processes and implications for satellite-based CCN estimates, *Atmos. Chem. Phys.*, *5*, 7585–7604, doi:10.5194/acp-15-7585-2015.
- Stelson, A., and J. H. Seinfeld (1982), Relative humidity and pH dependence of the vapor pressure of ammonium nitrate-nitric acid solutions at 25°C, *Atmos. Environ.*, *16*, 2507–2514.
- Textor, C., et al. (2006), Analysis and quantification of the diversities of aerosol life cycles within AeroCom, *Atmos. Chem. Phys.*, *6*, 1777–1813.
- Titos, G., A. Jefferson, P. J. Sheridan, E. Andrews, H. Lyamani, L. Alados-Arboledas, and J. A. Ogren (2014), Aerosol light-scattering enhancement due to water uptake during the TCAP campaign, *Atmos. Chem. Phys.*, *14*, 7031–7043, doi:10.5194/acp-14-7031.
- Virkkula, A., N. C. Ahlquist, D. S. Covert, W. P. Arnott, P. J. Sheridan, P. K. Quinn, and D. J. Coffman (2005), Modification, calibration and a field test of an instrument for measuring light absorption by particles, *Aerosol Sci. Technol.*, *39*, 68–83.
- Yang, W., A. Marshak, T. Várnai, and R. Wood (2014), CALIPSO observations of near-cloud aerosol properties as a function of cloud fraction, *Geophys. Res. Lett.*, *41*, 9150–9157, doi:10.1002/2014GL061896.
- Zhang, L., J. Y. Sun, X. J. Shen, Y. M. Zhang, H. C. Che, Q. L. Ma, Y. W. Zhang, X. Y. Zhang, and J. A. Ogren (2015), Observations of relative humidity effects on aerosol light scattering in the Yangtze River Delta of China, *Atmos. Chem. Phys.*, *15*, 8439–8454, doi:10.5194/acp-15-8439-2015.
- Ziemba, L. D., et al. (2013), Airborne observations of aerosol extinction by in situ and remote-sensing techniques: Evaluation of particle hygroscopicity, *Geophys. Res. Lett.*, *40*, 417–422, doi:10.1029/2012GL054428.
- Zieger, P., R. Fierz-Schmidhauser, E. Weingartner, and U. Baltensperger (2013), Effects of relative humidity on aerosol light scattering: Results from different European sites, *Atmos. Chem. Phys.*, *13*, 10,609–10,631, doi:10.5194/acp-13-10609.